#### ARTICLE IN PRESS

Journal of Alloys and Compounds xxx (xxxx) xxx



Contents lists available at ScienceDirect

### Journal of Alloys and Compounds

journal homepage: http://www.elsevier.com/locate/jalcom



## Mechanical properties of FeMnCoCr high entropy alloy alloyed with C/Si at low temperatures

Fei Yang <sup>a</sup>, Liming Dong <sup>b, \*</sup>, Lei Cai <sup>c</sup>, Xianjun Hu <sup>d</sup>, Feng Fang <sup>a, \*\*</sup>

- <sup>a</sup> Jiangsu Key Laboratory of Advanced Metallic Materials, Southeast University, Nanjing, 211189, China
- <sup>b</sup> School of Automotive Engineering, Changshu Institute of Technology, Changshu, 215500, China
- <sup>c</sup> Sunnywell (China) New Material Technology Co. Ltd, Changzhou, 213200, China
- <sup>d</sup> Jiangsu Sha-Steel Group, Zhangjiagang, 215625, China

#### ARTICLE INFO

# Article history: Received 21 August 2020 Received in revised form 7 November 2020 Accepted 8 November 2020 Available online xxx

Keywords:
High entropy alloy
Twinning induce plasticity
Geometrically necessary dislocations
Work hardening rate

#### ABSTRACT

Microstructural evolution and mechanical properties of FeMnCoCr high entropy alloy containing C and Si at various temperatures were investigated. The experimental results demonstrate that the microstructure of the HEAs alloy is a single-phase face-centered cubic solid solution, and the C and Si are completely dissolved in the matrix. The stacking fault energy of the alloy is about 33.96 mJ/m². Therefore, twins will be easy to form during the deformation process. Benefit from the synergistic effect of solid solution strengthening and twinning induced plasticity, the alloy shows a trade-off between high strength and good plasticity. Ultimate tensile strength of 757 MPa and considerable fracture ductility of 60.5% is obtained at room temperature. As the deformation temperature decreased to 227 K, the strength and plasticity are increased to 907 MPa and 69.6%, respectively. Under the low temperature, primary mechanical twins are suppressed, and more geometrically necessary dislocations and secondary nanoscale twins could be observed. The HEAs show a high work-hardening rate, which is related to dislocation slip being hindered by primary and secondary nano-twins.

© 2020 Elsevier B.V. All rights reserved.

#### 1. Introduction

Exploring strong and durable materials is essential for reducing weight, and, hence, energy consumption [1,2]. However, strength and plasticity are generally exclusive in metallic structural materials [3]. The addition of trace alloying elements can improve the strength of the materials, but leads to the precipitation of intermetallic compounds, thus deteriorating mechanical performance. High-entropy alloys (HEAs) have attracted extensive attention, as they have opened up a new field of synthesis strategy [4]. HEAs refer to a new alloy system composed of four or more elements in equiatomic or near-equiatomic ratios. The formation of intermetallic compounds is suppressed and tends to form a simple single-phase solid solution due to the large mixing entropy. HEAs have been found to possess a variety of unique properties, such as biocompatibility [5] and magnetic properties [6]. Apart from that, benefit from its good plasticity, wear resistance, corrosion

resistance and high-temperature softening resistance, HEA has a good application prospect as an engineering material [7,8]. Among the various types of HEAs, face centered cubic (FCC) HEAs have been the most widely studied due to their excellent fracture toughness [9,10]. Meanwhile, a low initial strength hindered their employment as a candidate for mechanical load-bearing parts. Severe plastic deformations, such as cold rolling, drawing, and high-pressure torsion [11], will increase the strength obviously, but also damage the plasticity, while introducing complex processing. Therefore, it is of great practical significance to develop a cast-HEA with high strength and plasticity.

Ritchie et al. [12] revealed the mechanical performance of CrMnFeCoNi HEA at low and cryogenic temperatures, considering that higher strain-hardening at 77 K results from the triggering of mechanical nano-twinning. As one of the main deformation mechanisms in FCC metals, mechanical twinning plays an important role in deformation behaviour [9,13]. It acts as an obstacle to

https://doi.org/10.1016/j.jallcom.2020.157876 0925-8388/© 2020 Elsevier B.V. All rights reserved.

Please cite this article as: F. Yang, L. Dong, L. Cai *et al.*, Mechanical properties of FeMnCoCr high entropy alloy alloyed with C/Si at low temperatures, Journal of Alloys and Compounds, https://doi.org/10.1016/j.jallcom.2020.157876

<sup>\*</sup> Corresponding author.

<sup>\*\*</sup> Corresponding author. School of Materials Science and Engineering, Southeast University, Jiangning District, Nanjing, 211189, China. E-mail addresses: donglm@cslg.edu.cn (L. Dong), fangfeng@seu.edu.cn (F. Fang).

F. Yang, L. Dong, L. Cai et al.

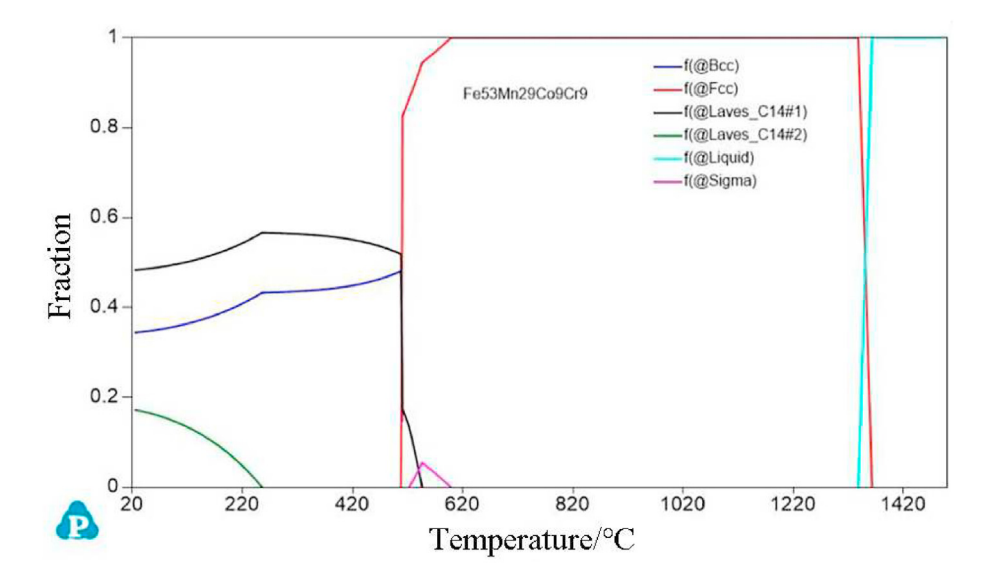


Fig. 1. Phase diagram for Fe<sub>53</sub>Mn<sub>29</sub>Co<sub>9</sub>Cr<sub>9</sub> HEA calculated by Pandat software.

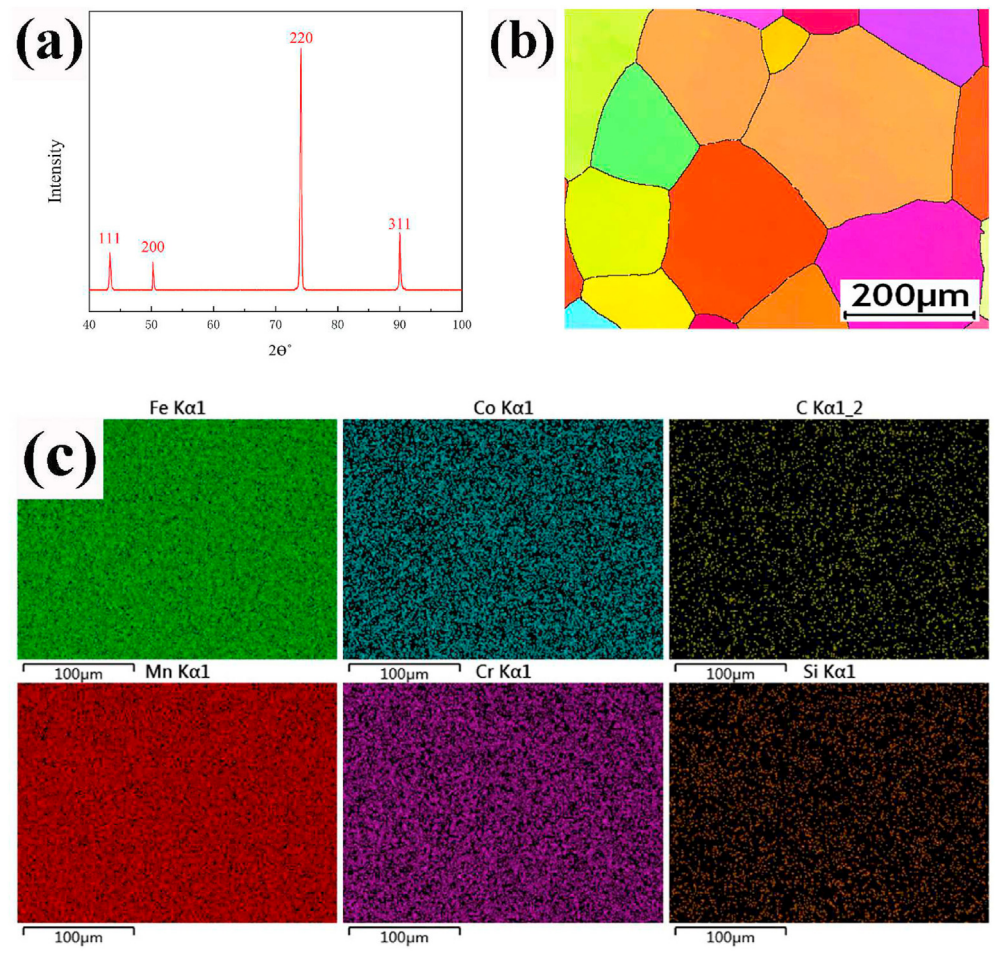
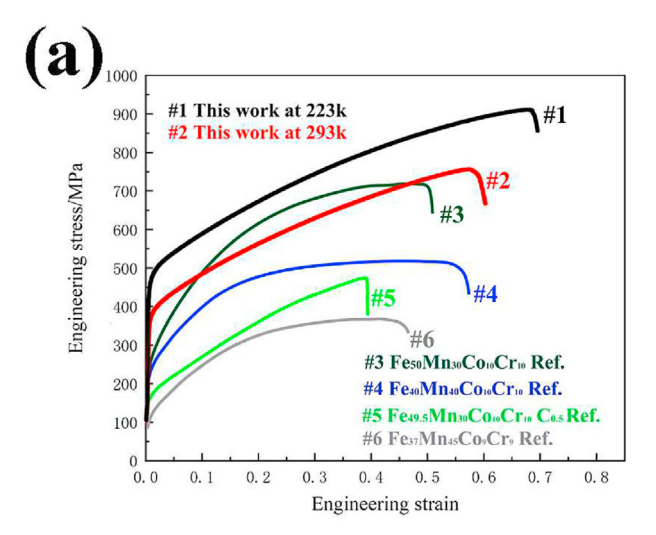


Fig. 2. (a) XRD patterns, (b) EBSD image, (c) element distribution.

dislocation slip, reducing the path of movement and increasing the density of dislocations [14]. Raabe et al. attributed the high strainhardening rate of twinning-induced plasticity (TWIP) steel to the interaction between dislocations and mechanical twins as well [15,16]. Generally, the incidence of mechanical twins depends on the stacking-fault energy (SFE), and the nucleation frequency increases with decreasing SFE [17-19]. The deformation mechanism transforms from dislocation slip (SFE  $\geq$  40 mJ/m²) to dislocation slip plus deformation twin (20 mJ/m²  $\leq$  SFE  $\leq$  40 mJ/m²) and dislocation slip plus martensitic transformation (SFE < 20 mJ/m<sup>2</sup>) [20]. A similar strengthening mechanism has also been introduced into HEAs. The Fe<sub>80-X</sub>Mn<sub>X</sub>Co<sub>10</sub>Cr<sub>10</sub> series of HEAs were originally proposed for tailoring the SFE by adjustment of the Mn content. Then, transformation-induced plasticity (TRIP) or TWIP becomes dominant during the deformation procedure [21,22]. The results show that FeMnCoCr alloys possess better comprehensive mechanical behaviour compared to traditional alloys and previously reported HEAs. For example, the ultimate tensile strength (UTS) of Fe<sub>50</sub>Mn<sub>30</sub>Co<sub>10</sub>Cr<sub>10</sub> dual-phase HEA was increased from 720 MPa to 870 MPa with decreasing average grain size from 45 mm to 4.5 mm, also the total elongation (TE) increases from 52% to 73% due to the promotion of phase transformation through grain refinement [23]. It has been proved that the strength of FeMnCoCr can be



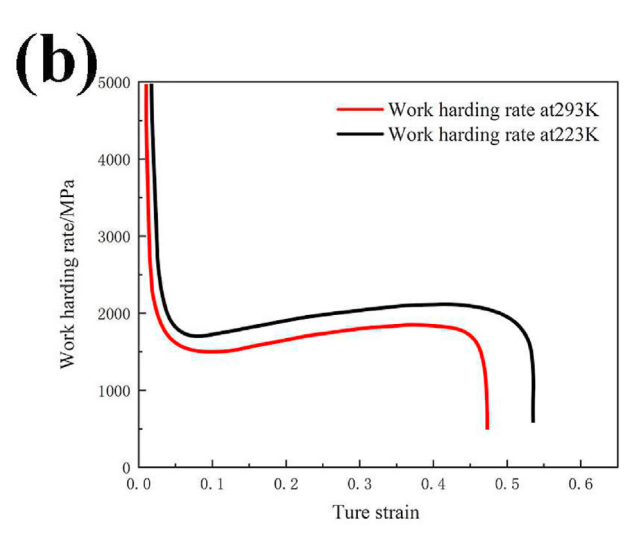


Fig. 3. (a) Engineering stress-strain curve, (b) Work hardening rate versus true strain curve.

improved by the alloying of interstitial elements such as carbon [24,25]. Li [26] reported an increase in the UTS from 870 MPa to 960 MPa after the addition of 0.5% carbon to  $Fe_{50}Mn_{30}Co_{10}Cr_{10}$  with little sacrifice in plasticity. Jian Chen et al. [27] found that C in HEAs can easily combine with Cr to form M<sub>3</sub>C<sub>7</sub> carbides [25,28], and that precipitation strengthening is produced. The interstitial strengthening of C can be summarized as follows: increasing stacking fault energy and improving phase stability [23,29,30], providing higher lattice distortion and friction stress compared to those of a substitutional solid solution [31-33]. As one of the common nonmetallic elements, the effect of alloying with Si on mechanical performance is also worth studying [34]. After adding 1.5% (wt.%) Si to the Fe-18Mn-0.6C (wt.%) TWIP steel [35], the yield strength can be increased from 387 MPa to 452 MPa due to the Si solid solution in the FCC austenite. Liu [36] and Kumar [37] et al. observed that with increased Si content in Al<sub>0.5</sub>CoCr-CuFeNiSix and AlCoCrCuFe-NiSix HEAs the structure changed from single-phase FCC to dualphase FCC-BCC, and the hardness was greatly improved. The effect of Si addition on the SFE has been analysed [38], and the SFE for Fe–Mn steel was found to decrease by 1.3 mJ/m<sup>2</sup> with the addition of 1% (at%) Si. Considering that the structure and composition of FeMnCoCr is similar to that of Fe—Mn steel [22], alloying Si can not only produce solution strengthening but can also reduce SFE, making it easier to trigger deformation twins or even secondary nano-twins. According to the above analysis, if a proper amount of C and Si elements is added into an FeMnCoCr alloy, one can, on the one hand, prepare a novel casting material with high strength and plasticity, benefiting from the interstitial solution, substitutional solution, and twin-induced plasticity. On the other hand, the alloying of HEAs mainly focuses on a single element solution (such as C, Al, B, rare earth elements) [13], while less attention is paid to a dual-element solution, especially non-metallic elements. This experiment can make up for the scarcity of related research.

In the present work, Fe<sub>53</sub>Mn<sub>29</sub>Co<sub>9</sub>Cr<sub>9</sub> HEAs was selected as the target material, the corresponding phase diagram calculated by Pandat is shown in Fig. 1. The casting is a single-phase FCC structure at room temperature. To avoid the precipitation of intermetallics, the addition of C was controlled at 1%, and a small amount of Si (1%) was added on this basis. The SFE was calculated by JMatPro to be approximately 37.4 mJ/m², slightly lower than the threshold value for twinning (40 mJ/m²) [19,20]. For convenience, the dual-element C/Si alloying with FeMnCoCr high-entropy alloys will be defined later as De-HEAs. The microstructure of the De-HEAs casting was systematically studied. Tensile tests were carried out at two different temperatures (223 K and 293 K), and the effect of deformation temperature on the microstructure, mechanical properties and twinning activity was analysed.

#### 2. Experiment and methods

Firstly, 1% of C and Si elements were added into Fe $_{53}$ Mn $_{29}$ Co $_{9}$ Cr $_{9}$  high entropy alloys, in the form of a master alloy with Fe. An ingot with a size of  $\Phi 100 \times 20 \text{ mm}^3$  was prepared by vacuum induction melting in an Ar atmosphere. The purity of each raw material is above 99.9%. The acquired ingots were annealed at 1200 °C for 6 h in a low vacuum melting furnace (1  $\times$  10 $^{-2}$  Pa) followed by water quenching for homogenization. The crystal structure of the ingot was characterized by X-ray diffraction with Cu K $\alpha$  radiation (XRD, Bruker D8); the measurement deviation for the instrument was corrected by using fully annealed silicon powder, the scattering angle is from 40 to 100°. Flat dog-bone shaped specimens with gauge dimensions of 15 mm  $\times$  2 mm  $\times$  1.5 mm were manufactured from the ingot by electric discharge machine (EDM). Both sides of the tensile specimen were sanded to eliminate the oxide layer and trace produced during annealing and EDM. Strength and plasticity

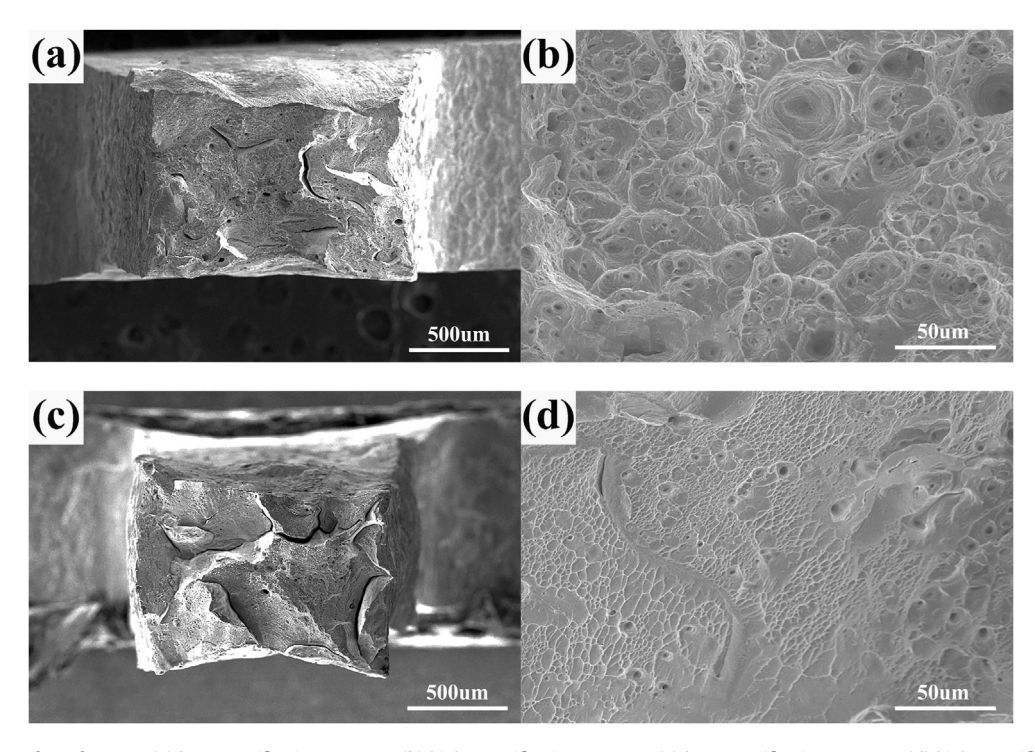


Fig. 4. Fracture surfaces for HEAs (a) low magnification at 293 K, (b) high magnification at 293 K, (c) low magnification at 223 K, (d) high magnification at 223 K.

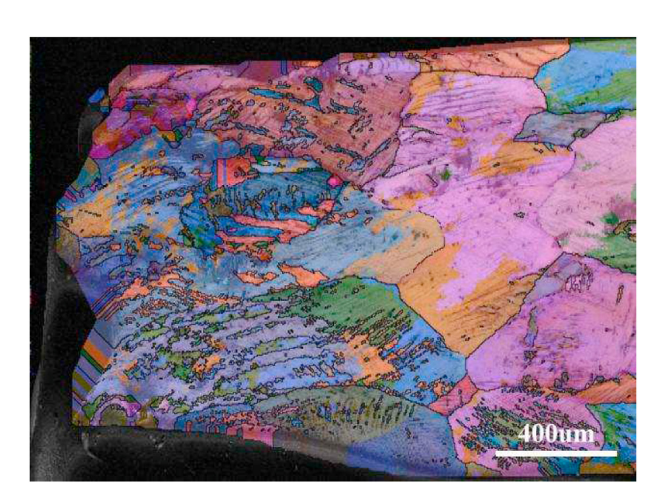


Fig. 5. EBSD near a fracture at 223 K.

are characterized by uniaxial tensile testing machine (MTS CMT 5105)), equipped with incubator, and stress-strain curve is recorded by extensometer at room temperature. Since the extensometer cannot be used at 223 K, the strain must be measured indirectly by the displacement of the beam. Three specimens for each sample were tested with a strain rate of  $1 \times 10^{-3}$  at room and low temperatures (293 K and 223 K). The fracture morphology and grain orientation were examined by field emission scanning electron microscopy (FE-SEM, FEI Sirion) equipped with electron backscatter diffraction (EBSD) and energy dispersive X-ray spectroscopy (EDS). The microstructures were analysed in detail by transmission electron microscopy (TEM, FEI Tecnai G2), operating at an acceleration voltage of 200 kV. For the preparation of TEM samples, a thin slice was first sanded to a thickness of approximately 100 µm, and a disc with a diameter of 3 mm was punched out of the slice. Then, the disc was mechanically polished to a thickness of 30  $\mu\text{m}\text{,}$  and an ion-beam was used to thin the perforation at 100 K. Nano-indentation measurements (Agilent Nano indenter, G200) were conducted to test the hardness of the microstructure near the tensile fracture; the load-displacement curve was acquired, and a holding time of 15 s was applied at the peak load above 10 mN. Each sample was tested 5 times at 5  $\mu$ m intervals to avoid any overlap of plastic zones created by neighboring indentations. Before the test, the samples were electropolished to remove the stress layer on the surface and ensure the accuracy of the measurement.

#### 3. Results and discussion

#### 3.1. Microstructure of homogenized HEAs

The XRD patterns obtained for the homogenized alloy are shown in Fig. 2a. The single-phase FCC structure was detected, and no obvious intermetallic compounds were formed, indicating that C and Si exist in the matrix as solution atoms. Fig. 2b shows the phase structure, the resolution of the FCC phase is 99.8%. No second phase is observed, which is consistent with the discovery reflected by the XRD. On account of the EBSD result, the measured grain size was determined to be approximately 200  $\mu m$ . As shown in Fig. 2c, all elements are evenly distributed in the matrix without obvious segregation.

In addition to the preliminary prediction for the SFE through simulation software, it is also necessary to calculate the true SFE through detection [35,38,39]:

$$\gamma = \frac{K_{111}\omega_0 G_{111}\alpha_0 A - 0.37}{\pi\sqrt{3}} \frac{\varepsilon^2}{\alpha}$$
 (1)

where  $K_{111}\omega_0$  represents the proportional constant of 6.6,  $\alpha_0$  is the lattice constant and A is related to the anisotropy with a value of 3.43; G is the shear modulus in the (111) plane, which is approximately 81 GPa;  $\varepsilon$  is the micro-strain determined from a Willamson-Hall plot obtained from the XRD profiles [40];  $\alpha$  is the frequency of

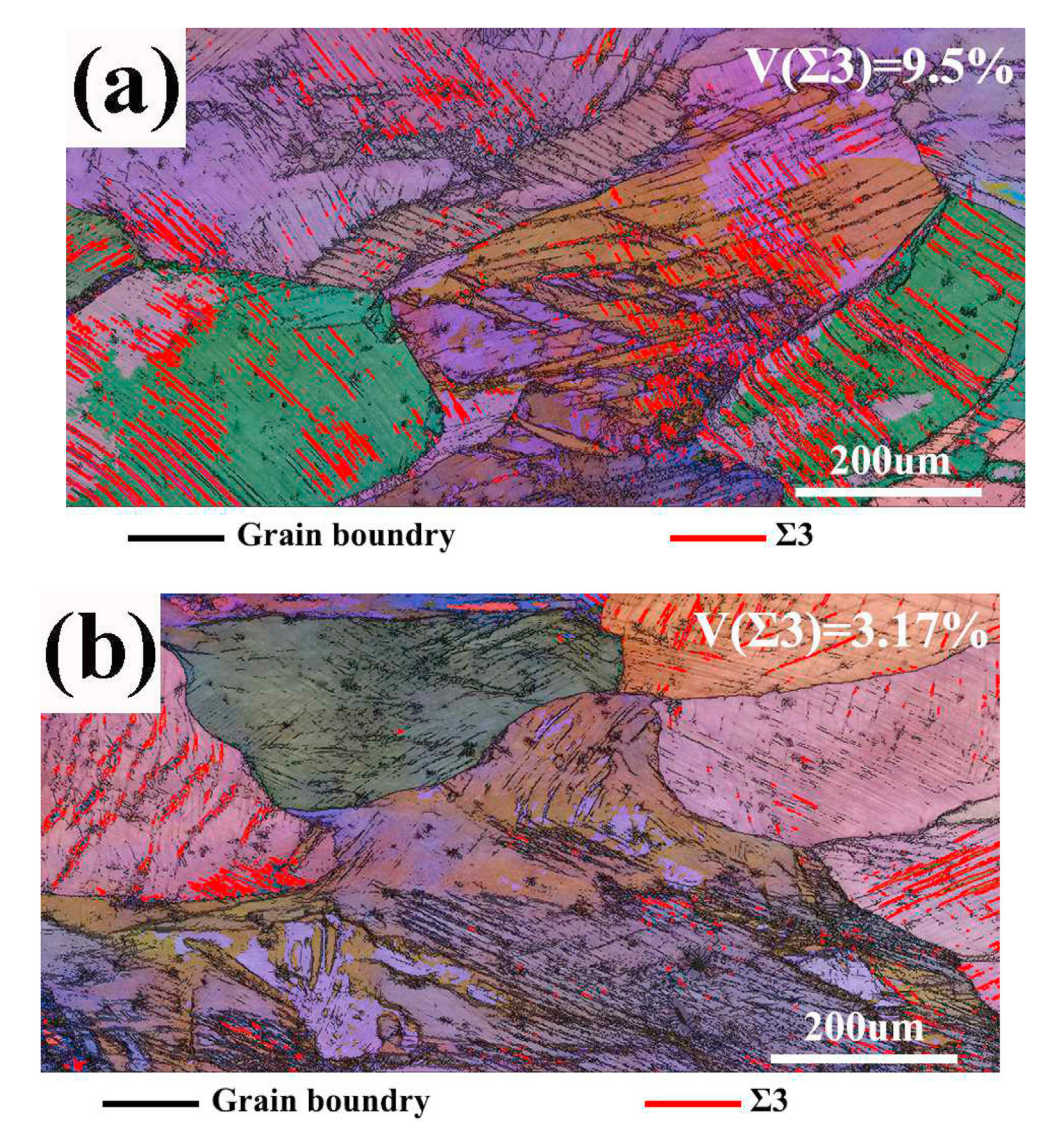


Fig. 6. EBSD near a tensile fracture (a) At 293 K, (b) At 223 K.

the stacking fault, which is measured for strain free (0%) and 5% strained samples; the relevant formula is expressed as follows [38]:

$$\begin{split} \Delta 2\theta &= (2\theta_{200} - 2\theta_{111})_{5\%} - (2\theta_{200} - 2\theta_{111})_{0\%} \\ &= -\frac{45\sqrt{3}}{\pi^2} \left( tan\theta_{200} + \frac{1}{2}\theta_{111} \right) \alpha \end{split} \tag{2}$$

where  $\theta_{hkl}$  represents the peak position for the {hkl} plane in the XRD. According to formula 1 and 2, the SFE for De-HEA is 33.96 mJ/m². The actual value is lower than the simulated value of 37.4 mJ/m² calculated by JmatPro, which may be related to the composition deviation for the solid solution element.

#### 3.2. Mechanical properties of the HEAs

Fig. 3a shows the engineering stress-strain curves obtained for De-HEAs. Compared with previously reported FeMnCoCr alloys [15,23,29,41], the micro-alloying of C and Si elements greatly improves the strength and maintains the moderate ductility. At room temperature, when the true strain is 0.4, the strain hardening rate reaches a maximum of 1825 MPa (Fig. 3b), approximately G/43 (G is

the shear modulus), close to the value range for TWIP Steel (G/20-G/40) and much higher than that for traditional FCC metal (G/200) [13]. Compared with traditional metal materials, the strength and elongation of the alloy are greatly improved with decreasing test temperature. At 223 K, the ultimate tensile strength is increased to 907 MPa and the fracture elongation is 69.6%. The strain hardening of De-HEAs increases with decreasing temperature, indicating that dislocation slip is more difficult, and needs to bear more stress to produce a corresponding deformation. It can be concluded that the De-HEAs has a low ductile brittle transition temperature (DBT).

#### 3.3. Microstructure evolution of the HEAs

Fig. 4 reveals the fracture morphology of De-HEAs after tensile deformation. At 293 K, necking occurs accompanied by the formation of secondary cracks (Fig. 4a). Many uniform dimples were observed at high magnification (Fig. 4b), implies excellent ductility. At 223 K, more secondary cracks connected with each other, showing a similar intergranular fracture morphology (Fig. 4c). The dimples observed at high magnification are shallow and small (Fig. 4d). To verify the low temperature fracture mechanism, an EBSD test was carried out near the fracture, as shown in Fig. 5. The

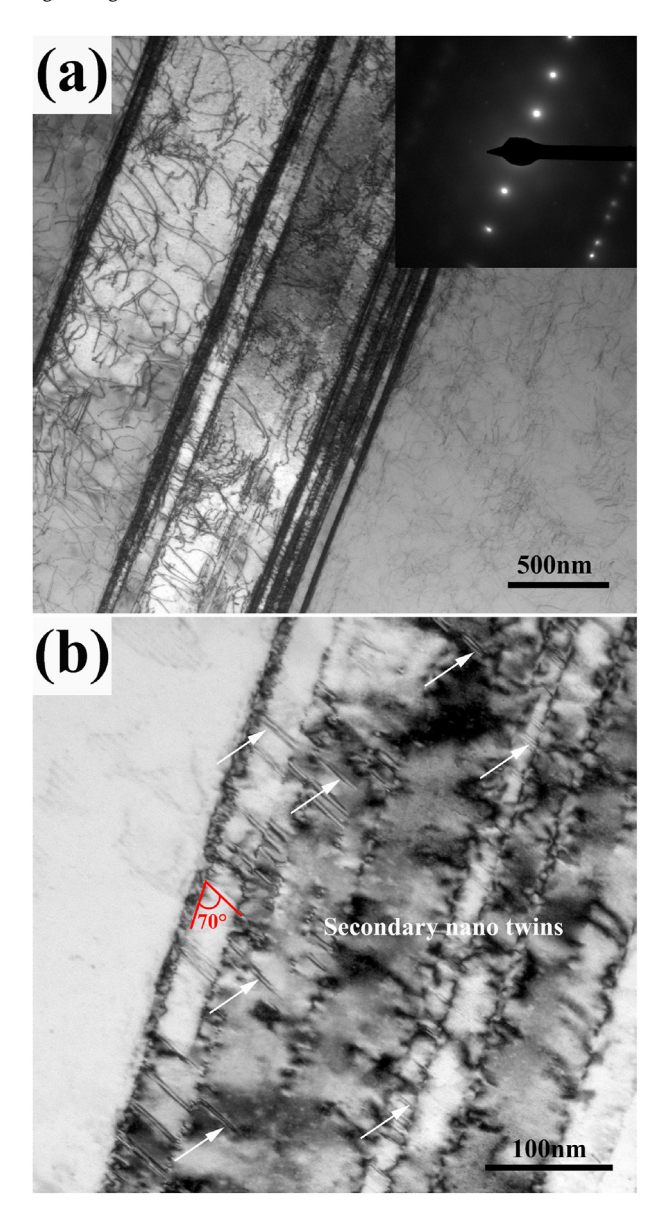


Fig. 7. Tensile structure at 293 K (a) Primary mechanical twins, (b) Secondary nanotwins.

black line in the figure represents the grain boundary, no obvious grain boundary trace is observed at the crack source, illustrating the

fact that the failure is still dominated by a transgranular fracture.

Fig. 6 shows the EBSD detected at a uniform plastic deformation area. After tensile deformation, the original equiaxed crystal is severely stretched. Through statistical analysis of the volume fraction of twin boundaries ( $\Sigma 3$ ),  $V_{\Sigma 3}$  is determined to be only 3.17% at 223 K, which is much lower than that of 9.5% at 293 K. It is generally believed that twinning in the process of deformation will trigger TWIP, so that the alloy can withstand greater deformation and obtain better plasticity. According to previous study [12,14,42], better ductility at cryogenic temperatures is associated with the formation of a large number of twins. However, the underlying reason for the high strength and plasticity of De-HEAs at low temperature cannot be derived from fracture morphology and EBSD test results alone. Therefore, it is necessary to explore the relationship between the high strength, elongation and deformation mechanism through in-depth analysis of the microstructure.

TEM images of the mechanical twins in the De-HEAs after tensile deformation at 293 K are shown in Fig. 7. A large number of primary mechanical twins are formed in the matrix, and there is a dense dislocation accumulation between the primary twins. These results show that the twins can be used as a special grain boundary to refine the grains and have an important effect on the dislocation slip. The relevant strengthening effect can be explained by the Hall-Petch formula [9]. Observed at high magnification, intensive secondary nano-twins (as indicated by the white arrow) are generated inside the primary twins (Fig. 7b) that are arranged at an angle of 70° with the primary mechanical twins, which is in good agreement with the calculated angle between the  $[11\overline{1}]$  and  $[\overline{1}1\overline{1}]$  directions [35,43]. Due to the solution strengthening of C and Si atoms in De-HEAs, dislocation-dominated plastic slip becomes more difficult, and the critical stress required to activate a twin can be more easily obtained in the early stage of deformation. Once the critical twin stress is reached, the primary twin nucleates at the grain boundary. With increasing strain, a large number of twins are formed that begin to cluster, following which the secondary twinning system begins to activate. Due to the interaction of solution atoms, primary deformation twins and secondary nanotwins, a combination of high strength and plasticity is obtained for De-HEAs at room temperature.

Fig. 8 shows a schematic diagram for the evolution of the De-HEAs structure under different tensile strains. For the convenience of illustration, the grain deformation during the tensile process is ignored. The deformation under low strain is dominated by dislocation slip, and the deformation mechanism changes from dislocation slip to TWIP upon reaching the critical twin stress. At high strain, the secondary nano-twins start to activate, and the formation of a large number of nano-twins results in a more obvious effect on the grain refinement strengthening of the alloy,

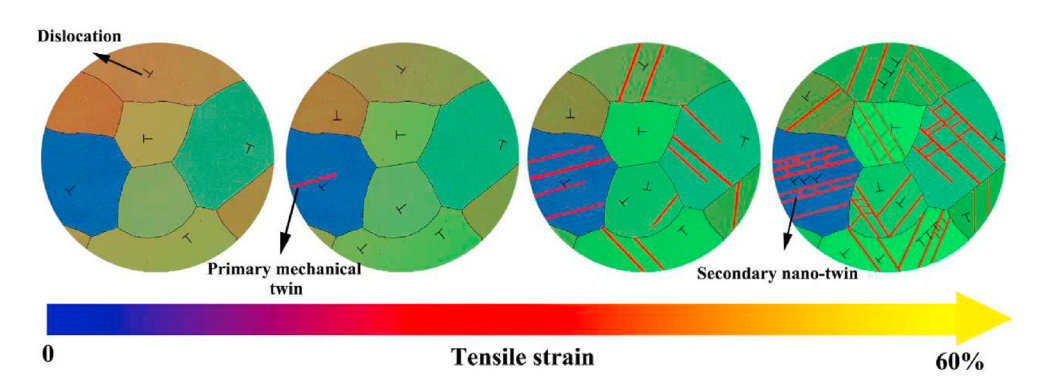


Fig. 8. Diagrammatic sketch of deformation at 293 K.

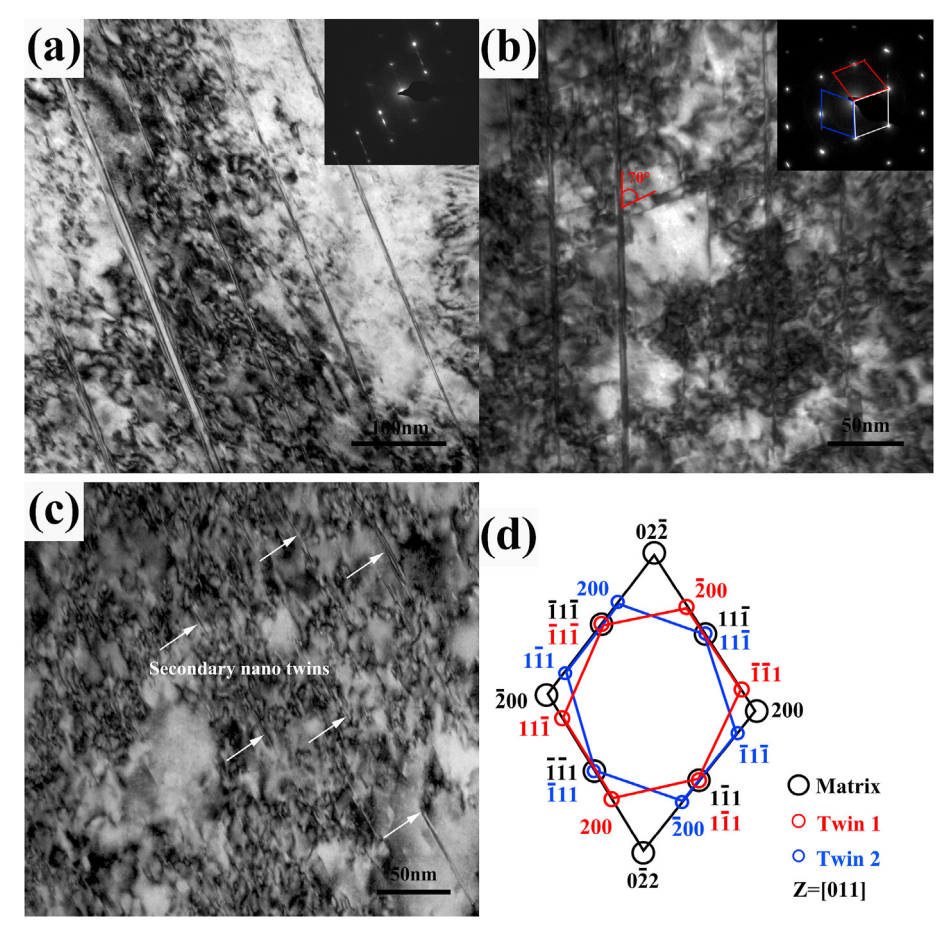


Fig. 9. Tensile structure at 223 K (a) Primary mechanical twins, (b) and (c) Secondary nano-twins, (d) the corresponding index results.

which leads to a continuous increase in the work-hardening rate.

After the application at 223 K, the size and volume fraction of the primary twins are significantly reduced, as shown in Fig. 9a. Compared with the deformed structure at room temperature, secondary nano-twins were extensively discovered to not only exist in the primary twins but were also found to appear in the high-density dislocation group (Fig. 9b and c), the calibration for the diffraction pattern is shown in Fig. 9d. The deformation temperature affects the twinning ability in several different ways [14,43]. On the one hand, similar to a traditional alloy, there is a critical stress that needs to be overcome in order to activate secondary nano-twins. At higher temperatures (e.g., 293 K), it becomes more difficult to achieve this stress due to lower tensile strength or dynamic recovery. When the deformation temperature decreases (e.g., to 223 K), the dynamic recovery is restrained and the tensile strength increases (Fig. 3), making it easier to reach critical stress at lower strain. On the other hand, He [44,45] reported that the SFE decreases with decreasing temperature. A lower SFE means that it is easier to trigger twinning and even phase transformation during deformation. Jeong [35] reported that the volume fraction of primary mechanical twins is increased almost linearly with decreasing SFE (from 30 mJ/m<sup>2</sup> to 20 mJ/m<sup>2</sup>), with a slight increase found at low SFE (below 20 mI/m<sup>2</sup>). However, secondary nano-twins were found to rapidly increase for an SFE of less than 20 mJ/m<sup>2</sup>, resulting in additional strain hardening. From the plane slip dislocation slip at room temperature to the mechanical nano-twin at low temperature, strain hardening is continuous and stable. Apart from that, the deformation twins contain a high density of inherent dislocations, which act as a strong barrier for dislocation sliding and

further promote strain hardening [46]. It can be seen that the secondary nano-twinning is one of the important deformation modes at low temperature. Due to the nanoscale size of the secondary twins, they are hard to detect through EBSD, which can explain the statistical deviation observed for the twin boundary volume fraction.

The strain hardening curve for traditional metal materials decreases monotonously with increasing strain. In this work, (Fig. 3b), a higher strain hardening rate is obtained at low temperature. When the true strain reaches 5%, the strain hardening begins to slowly increase, which is related to the transformation of the deformation mechanism from dislocation slip to deformation twin. At the same time, twinning can change the orientation of the crystal from an unfavourable orientation to a new favourable orientation, following which slip and crystal deformation occurs again [13], so that the dislocation density is further increased. TEM analysis shows that more secondary deformation twins are triggered at low temperature deformation, resulting in a higher strain hardening.

The distribution of dislocations has a great influence on the mechanical properties of HEAs. In crystalline materials, dislocations can be divided into statistical storage dislocations (SSD) and geometrically necessary dislocations (GND) [47]. Generously, GND is used to characterize the degree of plastic deformation. The density of GND in De-HEA after deformation at different temperatures was analysed, and the kernel average misorientation (KAM) was used to expound the intragranular misorientation introduced by GND [48]. The averaged misorientation between the adjacent EBSD measurement points can be used as a method to measure the

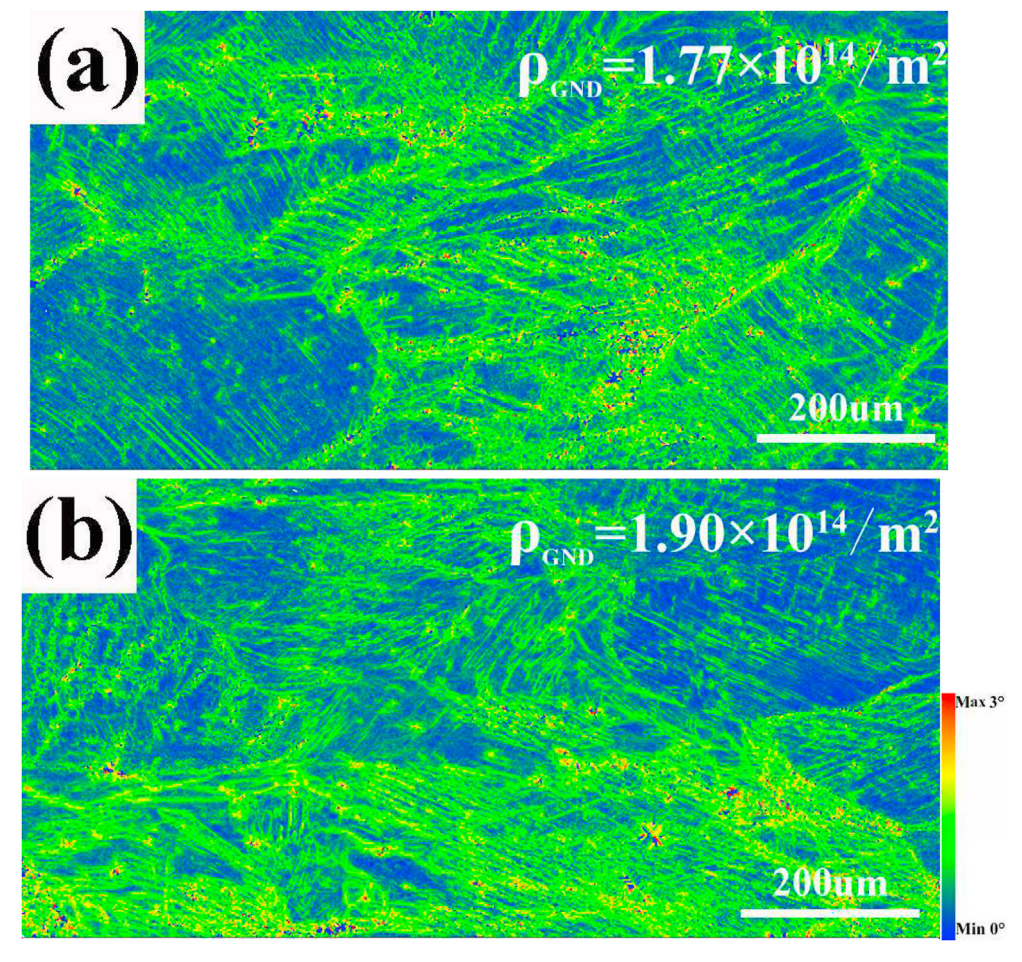


Fig. 10. KAM map after tensile testing at (a) 293 K, (b) 223 K.

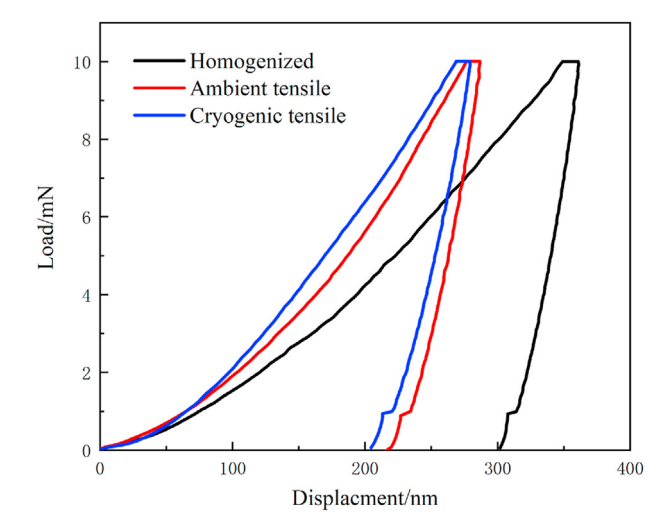


Fig. 11. Nano-indentation of fracture after tensile test.

approximate density of GND ( $\rho_{GND}$ ). A misorientation angle above 3° is attributed to the low (or high) angle grain boundary, hence, it is excluded from the GND calculation. Fig. 10a and b shows the KAM map corresponding to the deformed microstructure shown in Fig. 6a and b, respectively.

The  $\rho_{GND}$  is given by the product of the boundary plane area unit

volume and the dislocation line length per unit area, as follows [20,49]:

$$\rho_{GND} \approx \frac{\alpha \theta}{\mu b} \tag{3}$$

In the present work,  $\alpha$  was chosen to be 3 for boundaries of mixed character,  $\mu$  is the unit length as 1  $\mu$ m and b is the magnitude of the Burgers vector, 0.255 nm, and  $\theta$  is the average misorientation angle for the selected area, which can be calculated from the following formula:

$$\theta = \exp\left[\frac{1}{N}\sum_{1}^{i}\ln KAM_{i}\right] \tag{4}$$

where N represents the number of test area points and  $KAM_i$  is the local value of KAM at point i. The measured values for GND are listed in the upper right corner of the picture, the stress in the material in the process of deformation was evaluated (Fig. 10). The KAM identified by EBSD is not distributed in each sample evenly. The misorientation at the grain boundaries and twin boundaries (correspond to Fig. 6) is significantly higher than that inside the austenite matrix. Indicating that these two types of boundaries can not only be regarded as barriers for dislocation slip but also as one of the main factors giving rise to the emergence of GND. The higher strain hardening rate at lower temperature is attributed to an increase in the dislocation density and the interaction between dislocations and mechanical twins.

F. Yang, L. Dong, L. Cai et al.

Journal of Alloys and Compounds xxx (xxxx) xxx

Nano-indentation was utilized to probe the mechanical properties of a nanoscale structure after tensile testing. The load-displacement curves obtained are shown in Fig. 11. After homogenization, the nano-indentation hardness of the alloy was determined to be 5.4 GPa. The hardness of the structure deformed at 223 K was determined to be 9.4 GPa, which is slightly higher than the value of 8.8 GPa obtained at 293 K. The difference in the hardness value is closely related to the microstructure. In this work, the hardness value is mainly affected by nano-twins and dislocations, and the result is consistent with previous characterization and analysis [50,51].

It is concluded that primary deformation twins can be suppressed, but a higher density of dislocations and secondary nanotwins will be produced at low temperature. The propagation of dislocations results in work hardening, and the nano twinning induces grain refinement and twinning induced plasticity contribute to the improvement of plasticity. Hence, the strength and plasticity of the alloy is greatly enhanced simultaneously at low temperature. Inspired by this, if De-HEAs first suffers from deformation (rolled or drawn) at low temperature to fully develop the secondary nanotwin, then, from measurement of the mechanical performance at room temperature, one can determine whether or not the strength can be further improved and the high plasticity maintained. The relevant research deserves further attention in the future.

#### 4. Conclusion

Through reasonable composition design, a single-phase FCC structure can be maintained by adding one percent of C and Si elements to a  $Fe_{53}Mn_{29}Co_9Cr_9$  HEAs, and the stacking fault can be tailored below 33.96 m]/m<sup>2</sup>.

- The synergistic effect of solid solution strengthening and TRIP makes it easier to obtain excellent mechanical properties at room temperature, with strength of 757 MPa and elongation of 60.5%.
- 2) The De-HEAs exhibits a higher tensile yield strength of 907 MPa and a considerable percent elongation of 69.6% at 223 K. The tensile properties of the C/Si alloyed HEAs are greatly improved compared to that at 293 K.
- 3) Upon deformation at low temperature, primary deformation twins are suppressed, but a higher density of dislocations and secondary nano-twins are produced.
- 4) The strain hardening ability of the alloy is greatly improved due to the interaction between dislocations and twins. The dominant deformation mechanism changes from dislocation slip and primary mechanical twins at room temperature to secondary nano-twins at low temperature.

#### **CRediT authorship contribution statement**

**Fei Yang:** Executor of the experiment, Writing - original draft. **Liming Dong:** Designer of the experiment; Editing. **Lei Cai:** Analysis of research results. **Xianjun Hu:** Investigation, of microstructure. **Feng Fang:** Designer of the experiment; Editing, Supervision.

#### **Declaration of competing interest**

The authors declare that they have no known competing financial interests or personal relationships that could have appeared to influence the work reported in this paper.

#### Acknowledgement

This work is supported by the National Natural Science Foundation of China (grant no. 51371050), the Science and Technology Advancement Program of Jiangsu Province (BA2017112) and the 333 projects of Jiangsu Province, China (BRA2018045). The study was also partly supported by Industry-University Research Cooperation Project of Jiangsu Province, China (BY2018194).

#### References

- S.J. Zinkle, J.T. Busby, Structural materials for fission & fusion energy, Mater. Today 12 (2009) 12–19.
- [2] J.W. Lee, H.M. Baek, S.K. Hwang, I.-H. Son, C.M. Bae, Y.-T. Im, The effect of the multi-pass non-circular drawing sequence on mechanical properties and microstructure evolution of low-carbon steel, Mater. Des. 55 (2014) 898–904.
- [3] O. Robert Ritchie, The conflicts between strength and toughness, Nat. Mater. 10 (2011) 817–822.
- [4] Y.F. Ye, Q. Wang, J. Lu, C.T. Liu, Y. Yang, High-entropy alloy: challenges and prospects, Mater. Today 19 (2016) 349–362.
- [5] W.Y. Ching, S.R. San, J. Brechtl, R. Sakidja, M.Q. Zhang, P.K. Liaw, Fundamental electronic structure and multiatomic bonding in 13 biocompatible highentropy alloys, NPJ Comput. Mater. 6 (2020).
- [6] C. Chen, H. Zhang, Y. Fan, W. Zhang, F. Li, A novel ultrafine-grained high entropy alloy with excellent combination of mechanical and soft magnetic properties, J. Magn. Magn Mater. 502 (2020) 166513.
- [7] Z. Yong, T.T. Zuo, T. Zhi, M.C. Gao, K.A. Dahmen, P.K. Liaw, P.L. Zhao, Microstructures and properties of high-entropy alloys, Prog. Mater. Sci. 61 (2014) 1–93.
- [8] C.C. Zhao, A. Inoue, F.L. Kong, J.Y. Zhang, A.L. Greer, Novel phase decomposition, good soft-magnetic and mechanical properties for high-entropy (Fe0.25Co0.25Ni0.25Cr0.125Mn0.125)100-B (x = 9-13) amorphous alloys, J. Alloys Compd. (2020) 155917.
- [9] Z. Li, S. Zhao, R.O. Ritchie, M.A. Meyers, Mechanical properties of high-entropy alloys with emphasis on face-centered cubic alloys, Prog. Mater. Sci. 102 (2019) 296–345.
- [10] J. Brechtl, S. Chen, C. Lee, Y. Shi, P.K. Liaw, A review of the serrated-flow phenomenon and its role in the deformation behavior of high-entropy alloys, Metal. Open Access Metall. J. 10 (2020) 1101.
- [11] J.Y. He, H. Wang, H.L. Huang, X.D. Xu, M.W. Chen, Y. Wu, X.J. Liu, T.G. Nieh, K. An, Z.P. Lu, A precipitation-hardened high-entropy alloy with outstanding tensile properties, Acta Mater. 102 (2016) 187–196.
- [12] B. Gludovatz, A. Hohenwarter, D. Catoor, E.H. Chang, E.P. George, R.O. Ritchie, A fracture-resistant high-entropy alloy for cryogenic applications, Science 345 (2014) 1153–1158.
- [13] B.C. De Cooman, Y. Estrin, S.K. Kim, Twinning-induced plasticity (TWIP) steels, Acta Mater. 142 (2018) 283–362.
- [14] W. Huo, F. Fang, H. Zhou, Z. Xie, J. Shang, J. Jiang, Remarkable strength of CoCrFeNi high-entropy alloy wires at cryogenic and elevated temperatures, Scripta Mater. 141 (2017) 125–128.
- [15] Y. Deng, C.C. Tasan, K.G. Pradeep, H. Springer, A. Kostka, D. Raabe, Design of a twinning-induced plasticity high entropy alloy, Acta Mater. 94 (2015) 124–133.
- [16] G. Laplanche, A. Kostka, O.M. Horst, G. Eggeler, E.P. George, Microstructure evolution and critical stress for twinning in the CrMnFeCoNi high-entropy alloy, Acta Mater. 118 (2016) 152–163.
- [17] P. Sathiyamoorthi, J. Moon, J.W. Bae, P. Asghari-Rad, H.S. Kim, Superior cryogenic tensile properties of ultrafine-grained CoCrNi medium-entropy alloy produced by high-pressure torsion and annealing, Scripta Mater. 163 (2019) 152–156.
- [18] H. Idrissi, L. Ryelandt, M. Veron, D. Schryvers, P.J. Jacques, Is there a relationship between the stacking fault character and the activated mode of plasticity of Fe–Mn-based austenitic steels? Scripta Mater. 60 (2009) 941–944.
- [19] J.-K. Kim, B.C. De Cooman, Stacking fault energy and deformation mechanisms in Fe-xMn-0.6C-yAl TWIP steel, Mater. Sci. Eng., A 676 (2016) 216–231.
   [20] Z.F. He, N. Jia, D. Ma, H.L. Yan, Z.M. Li, D. Raabe, Joint contribution of trans-
- [20] Z.F. He, N. Jia, D. Ma, H.L. Yan, Z.M. Li, D. Raabe, Joint contribution of transformation and twinning to the high strength-ductility combination of a FeMnCoCr high entropy alloy at cryogenic temperatures, Mater. Sci. Eng., A 759 (2019) 437–447.
- [21] Z. Li, F. Körmann, B. Grabowski, J. Neugebauer, D. Raabe, Ab initio assisted design of quinary dual-phase high-entropy alloys with transformation-induced plasticity, Acta Mater. 136 (2017) 262–270.
- [22] Z. Li, C.C. Tasan, K.G. Pradeep, D. Raabe, A TRIP-assisted dual-phase high-entropy alloy: grain size and phase fraction effects on deformation behavior, Acta Mater. 131 (2017) 323–335.
- [23] Z. Li, K.G. Pradeep, Y. Deng, D. Raabe, C.C. Tasan, Metastable high-entropy dual-phase alloys overcome the strength-ductility trade-off, Nature 534 (2016) 227–230.
- [24] L. Guó, X. Ou, S. Ni, Y. Liu, M. Song, Effects of carbon on the microstructures and mechanical properties of FeCoCrNiMn high entropy alloys, Mater. Sci.

F. Yang, L. Dong, L. Cai et al.

Journal of Alloys and Compounds xxx (xxxx) xxx

- Eng., A 746 (2019) 356-362.
- [25] M.V. Klimova, A.O. Semenyuk, D.G. Shaysultanov, G.A. Salishchev, S.V. Zherebtsov, N.D. Stepanov, Effect of carbon on cryogenic tensile behavior of CoCrFeMnNi-type high entropy alloys, J. Alloys Compd. 811 (2019) 152000.
- [26] S.-M. Lee, S.-J. Lee, S. Lee, J.-H. Nam, Y.-K. Lee, Tensile properties and deformation mode of Si-added Fe-18Mn-0.6C steels, Acta Mater. 144 (2018) 738–747.
- [27] J. Chen, Z. Yao, X. Wang, Y. Lu, X. Wang, Y. Liu, X. Fan, Effect of C content on microstructure and tensile properties of as-cast CoCrFeMnNi high entropy alloy, Mater. Chem. Phys. 210 (2018) 136–145.
- [28] N.D. Stepanov, N.Y. Yurchenko, M.A. Tikhonovsky, G.A. Salishchev, Effect of carbon content and annealing on structure and hardness of the CoCrFeNiMnbased high entropy alloys, J. Alloys Compd. 687 (2016) 59–71.
- [29] Z. Li, C.C. Tasan, H. Springer, B. Gault, D. Raabe, Interstitial atoms enable joint twinning and transformation induced plasticity in strong and ductile highentropy alloys. Sci. Rep. 7 (2017) 40704.
- [30] A. Saeed-Akbari, J. Imlau, U. Prahl, W. Bleck, Derivation and variation in composition-dependent stacking fault energy maps based on subregular solution model in high-manganese steels, Metall. Mater. Trans. 40 (2009) 3076—3090.
- [31] J. Su, D. Raabe, Z. Li, Hierarchical microstructure design to tune the mechanical behavior of an interstitial TRIP-TWIP high-entropy alloy, Acta Mater. 163 (2019) 40–54.
- [32] Z. Wang, I. Baker, Z. Cai, C. Si, G. Wei, The effect of interstitial carbon on the mechanical properties and dislocation substructure evolution in Fe40.4Ni11.3Mn34.8Al7.5Cr6 high entropy alloys, Acta Mater. 120 (2016) 228–239.
- [33] N.D. Stepanov, D.G. Shaysultanov, R.S. Chernichenko, N.Y. Yurchenko, G.A. Salishchev, Effect of thermomechanical processing on microstructure and mechanical properties of the carbon-containing CoCrFeNiMn high entropy alloy, J. Alloys Compd. 693 (2017) 394–405.
- [34] S.M. Lee, I.J. Park, J.G. Jung, Y.K. Lee, The effect of Si on hydrogen embrittlement of Fe-18Mn-0.6C-xSi twinning-induced plasticity steels, Acta Mater. 103 (2016) 264–272.
- [35] K. Jeong, J.-E. Jin, Y.-S. Jung, S. Kang, Y.-K. Lee, The effects of Si on the mechanical twinning and strain hardening of Fe–18Mn–0.6C twinning-induced plasticity steel, Acta Mater. 61 (2013) 3399–3410.
- [36] X. Liu, W. Lei, L. Ma, J. Liu, J. Liu, J. Cui, On the microstructures, phase assemblages and properties of Al0.5CoCrCuFeNiSix high-entropy alloys, J. Alloys Compd. 630 (2015) 151–157.
- [37] A. Kumar, P. Dhekne, A.K. Swarnakar, M.K. Chopkar, Analysis of Si addition on phase formation in AlCoCrCuFeNiSix high entropy alloys, Mater. Lett. 188

- (2017) 73-76.
- [38] X. Tian, Y. Zhang, Effect of Si content on the stacking fault energy in γ-Fe-Mn-Si-C alloys: Part I. X-ray diffraction line profile analysis, Mater. Sci. Eng., A 516 (2009) 73–77.
- [39] A.J. Zaddach, C. Niu, C.C. Koch, D.L. Irving, Mechanical properties and stacking fault energies of NiFeCrCoMn high-entropy alloy, JOM (J. Occup. Med.) 65 (2013) 1780–1789.
- [40] G.K. Williamson, W.H. Hall, X-ray line broadening from filed aluminium and wolfram. Acta Metall. 1 (1953) 22—31.
- [41] Z. Li, D. Raabe, Influence of compositional inhomogeneity on mechanical behavior of an interstitial dual-phase high-entropy alloy, Mater. Chem. Phys. 210 (2018) 29–36.
- [42] F. Yang, L. Dong, X. Hu, X. Zhou, F. Fang, Z. Xie, J. Jiang, Microstructural features and tensile behaviors of a novel FeMnCoCr high entropy alloys, Mater. Lett. 275 (2020) 128154.
- [43] P. Chowdhury, D. Canadinc, H. Sehitoglu, On deformation behavior of Fe-Mn based structural alloys, Mater. Sci. Eng. R Rep. 122 (2017) 1–28.
- [44] S. Huang, W. Li, S. Lu, F. Tian, J. Shen, E. Holmström, L. Vitos, Temperature dependent stacking fault energy of FeCrCoNiMn high entropy alloy, Scripta Mater. 108 (2015) 44–47.
- [45] F. He, Z. Wang, Q. Wu, D. Chen, T. Yang, J. Li, J. Wang, C.T. Liu, J.-j. Kai, Tuning the defects in face centered cubic high entropy alloy via temperature-dependent stacking fault energy, Scripta Mater. 155 (2018) 134–138.
- [46] S. Huang, H. He, L. Wei, K. Dongyoo, L. Song, L. Xiaoqing, H.m. Erik, K.S. Kyun, V. Levente, Twinning in metastable high-entropy alloys, Nat. Commun. 9 (2018) 2381.
- [47] M. Seyed Salehi, N. Anjabin, H.S. Kim, Study of geometrically necessary dislocations of a partially recrystallized aluminum alloy using 2D EBSD, Microsc. Microanal. 25 (2019) 656–663.
- [48] D. Wallis, A.J. Parsons, L.N. Hansen, Quantifying geometrically necessary dislocations in quartz using HR-EBSD: application to chessboard subgrain boundaries, J. Struct. Geol. 125 (2019) 235–247.
- [49] Y. Takayama, J.A. Szpunar, Stored energy and taylor factor relation in an Al-Mg-Mn alloy sheet worked by continuous cyclic bending, Mater. Trans. 45 (2004) 2316–2325.
- [50] V. Maier-Kiener, B. Schuh, E.P. George, H. Clemens, A. Hohenwarter, Nanoindentation testing as a powerful screening tool for assessing phase stability of nanocrystalline high-entropy alloys, Mater. Des. 115 (2017) 479–485.
- [51] R.S. Ganji, P. Sai Karthik, S.R. Bhanu, K.V. Rajulapati, Strengthening mechanisms in equiatomic ultrafine grained AlCoCrCuFeNi high-entropy alloy studied by micro- and nanoindentation methods, Acta Mater. 125 (2017) 58–68.